Kinetics and Specificity of HEK293T Extracellular Vesicle Uptake using Imaging Flow Cytometry

Brian Jurgielewicz
University of Georgia https://orcid.org/0000-0001-9900-8077
Yao Yao (Yao.yao@uga.edu)
https://orcid.org/0000-0002-8851-7885
Steven L. Stice
University of Georgia

Research

Keywords: extracellular vesicles, selective uptake, HEK293T, imaging flow cytometry

Posted Date: February 14th, 2020

DOI: https://doi.org/10.21203/rs.2.23634/v1

Abstract

Background : Extracellular vesicles (EVs) are nanosized vesicles naturally secreted from cells responsible for intercellular communication and delivery of proteins, lipids, and other genetic material. Ultimately, EVs could provide innate therapeutic contents and loaded therapeutic payloads such as small molecules and gene therapy vectors to recipient cells. However, comparative kinetic measures that can be used to quantify and ultimately optimize delivery and uptake of EV payloads are lacking. We investigated both dose and time effects on EV uptake and evaluated the potential specificity of EV uptake to better understand the kinetics and uptake of human embryonic kidney (HEK293T) derived EVs. Results : Utilizing an imaging flow cytometry platform (IFC), HEK293T EV uptake was analyzed. HEK293T EV uptake was dose and time dependent with a minimum threshold dose of 6,000 EVs per cell at 4 hours of co-culture. HEK293T EV uptake was inhibited when co-cultured with recipient cells at 4°C or with pre-fixed recipient cells. By co-culturing HEK293T EVs with cell lines from various germ layers, HEK293T EVs were taken up at higher quantities by HEK293T cells. Lastly, human neural stem cells (hNSCs) internalized significantly more HEK293T EVs relative to mature neurons. Conclusions : Imaging flow cytometry is a quantitative, high throughput, and versatile platform to quantify the kinetics of EV uptake. Utilizing this platform, dose and time variables have been implicated to affect EV uptake measurements making standardization of in vitro and in vivo assays vital for the translation of EVs into the clinic. In this study, we quantified the selectivity of EV uptake between a variety of cell types in vitro and found that EVs were internalized at higher quantities by cells of the same origin. The characterization of HEK293T EV uptake in vitro, notably specificity, dose response, and kinetic assays should be used to help inform and develop EV based therapeutics.

Background

Extracellular vesicle research is a burgeoning field due to the therapeutic and diagnostic utility of natural and engineered EVs. EVs range from 50-1000 nm in diameter, are produced from all cell types, and enriched with transmembrane proteins including CD63, CD81 and CD9, lipids, proteins, and DNA, RNA, mRNA and microRNA (1–5). EV content, notably active mRNA and miRNA, has been implicated in modulation of recipient cells via de-novo translation and post translational regulation of target cells (4,6) Understanding and then modifying kinetic EV uptake and internalization will eventually lead to optimized delivery of EV contents to target cells with high enough concentrations to have a therapeutic benefit.

Once thought to be the “the garbage of the cells” EVs have been harnessed as an alternative to cell therapies due to many advantages including their biocompatibility, low immunogenicity and toxicity, ability for repeated dosing, various routes of administration, and potential to deliver drugs and genetic therapies (3). Our group has previously reported positive effects of neural stem cell derived EVs in both stroke and traumatic brain injury. In both murine and porcine stroke models, EVs improved tissue and functional recovery post stroke (3,7,8). We have also shown EVs to be neuroprotective with functional benefits in a rodent traumatic brain injury model (9). Despite these observed effects and future potential

of EVs, there is little understanding of EV uptake specificity and kinetics, which may hinder translation of EV therapeutics into the clinic.

EVs have also been engineered as transference vectors and loaded with therapeutic agents including gene therapies and chemical compounds. HEK293T cells have been used extensively as EV producer cells due to their rapid proliferation rates and ability to be easily manipulated to enhance EV contents or surface composition (10–13). HEK293T EVs were used to deliver chemotherapeutics and therapeutic protein constructs in a Schwannoma model (14). HEK293T EVs delivered miRNA therapeutics for breast cancer (15). Due to this abundant utilization of HEK293T EVs, we analyzed their kinetics and specificity in this study.

Selective or specific uptake refers to an EV's natural ability to target specific cell types. There is abundant evidence on the mechanisms of EV internalization with little consensus on uptake specificity. Often EVs exhibit selective uptake by similar recipient cells as their parent cells, epithelial cells internalize more epithelial derived EVs than other recipient cells (16,17) and mesenchymal stem cells (MSC) internalize a significantly greater amount of MSC derived EVs compared to other cell lines in vitro (17). However, other studies found that EVs are internalized by all cell types and display a non-selective biodistribution when administered in vivo (18,19). Despite the immense therapeutic potential and interest of EVs, there is a deficiency in the understanding of EV uptake specificity. By better understanding EV uptake specificity, we can appropriately choose EV producer cells that are selectively internalized by recipient cells of interest and thus improve the therapeutic applicability of EVs.

A potential reason for conflicting EV uptake results is the lack of standardization in measurement platforms, including analyses of dose and time effects. Recently, an International Society for Extracellular Vesicles (ISEV) group of experts, released a position paper emphasizing the need for analysis of dose and time, amongst other confounding factors on EV uptake (20). The group stated that 'one dose does not fit all,' and that dose may affect EV uptake or selectivity. Elevating doses of HEK293T EVs shifts the biodistribution pattern in vivo (21). Uptake profiles of serum derived EVs were significantly altered by dose (22). Additionally, co-incubation times of EVs with recipient cells ranging from 15 minutes to 48 hours (23,24) may alter uptake measurements. If adopted by EV researchers and industry, a quantifiable and reliable process to determine standard dose and time curves, to help identify the minimum effective dose may lead to more robust and useful studies.

Previously, researchers have used standard flow cytometry along with various forms of low throughput microscopy including confocal microscopy to analyze EV uptake (25–27). However, these technologies have several limitations. Confocal microscopy can be time consuming and subjective. Traditional flow cytometers have been designed to measure biological particles in the cellular range, cannot differentiate EV swarm or coincidence, and have increased noise due to triggering (28–31). As mentioned by the ISEV group, there is growing awareness of the physical limitations of traditional flow cytometry and highlight the demand for specialized flow cytometry with detection limits in the 100 nm range (20,28). Imaging flow cytometry (IFC) combines the high throughput quantitative nature of flow cytometry along with

fluorescence imaging technology which can resolve inherently small fluorescent particles, down to 100 nm in diameter (31). IFC capabilities lead to low noise/background, decreased swarming, and charged coupled devices for image clarity (30,32). These characteristics assist in developing a gating strategy for characterizing EVs and uptake with visual confirmation in a high throughput manner as an accurate and quantifiable EV uptake platform (29,30,33).

In this study, CD63-eGFP expressing HEK293T cells were utilized as the donor cell line for EV production due to their common usage in therapeutic development. The isolated fluorescent EVs were co-cultured with recipient cell lines including neural and endothelial cells. Uptake was quantified using IFC, resulting in a standardized platform to measure the important kinetic EV uptake and internalization features for in vitro cell systems. Further we provide data on a process to quantify uptake of fluorescent EVs uptake in differing conditions and cultured cell lines to elucidate selective EV uptake.

Materials And Methods

Cell Culture

Human embryonic kidney cells (HEK293T) were purchased from ATCC and cultured in DMEM containing 10% fetal bovine serum, 100 units/mL penicillin, 100ug/mL streptomycin. Human neural stem cells (hNSC), SH-SY5Y neural cells, C3A liver epithelial cells, human umbilical vein endothelial cells (HUVEC), and neurons were all cultured under standard conditions at 37 °C, 5% CO_2 prior to extracellular vesicle uptake assays.

EV Labeling and Isolation

CD63-eGFP plasmid DNA was obtained from Addgene (#62964). CD63-pEGFP C2 was a gift from Paul Luzio (Addgene plasmid #62964). HEK293T cells were cultured to 70% confluency in 10 cm dishes and 10ug plasmid DNA was transfected using Lipofectamine 2000 according to the manufacturer's instructions. 24-hours post transfection media was changed to standard HEK293T media devoid of fetal bovine serum and collected for 3 consecutive days. As previously described (3), HEK293T media was filtered through a 0.22 µm filter and enriched by ultrafiltration using a 100 kDa regenerated cellulose Amicon centrifugal filter units and washed twice with PBS++. EVs were concentrated to one mL and concentration and size distributions were measured on Nanosight NS300 by the manufacturer's protocol (Malvern, United Kingdom).

Uptake Assays

Recipient cell lines were seeded at 60% confluency in a 6-well plate for 24 hours under standard culture conditions. Standard media was changed to fetal bovine serum free (FBS-) media prior to extracellular vesicle co-culture. GFP-tagged EVs were administered to cells at varying doses and time points. After co-culture, cells were resuspended in 5% trypsin and concentrated to around one million cells per 50uL for flow cytometry.

ImageStreamX Acquisition

Acquisition was performed on the ImageStreamX Mark II Imaging Flow Cytometer (Luminex Corporation, Seattle, Washington) using the INSPIRE software. A minimum of 5,000–10,000 cell events were acquired. Brightfield images were collected on channel one and side scatter (785 N m) on channel six. Green fluorescent protein (GFP) was excited by 488 nm argon laser at 200 mW and fluorescence was collected on channel two (505–560 nm). 60x magnification was used on every sample along with a low acquisition rate for high sensitivity.

IDEAS Analysis

Data and image analyses were conducted using the IDEAS software (Luminex). The gating strategy is the following:

1. Focus gate was determined to eliminate cells that were not in the field of focus using the Gradient RMS value. 2. The focused cells were gated to eliminate doublets and debris using area brightfield vs aspect ratio brightfield. Gated data was used to create histograms and generate statistics references measuring fluorescence intensity (sum of all pixels in an image), maximum pixel intensity (intensity of the brightest pixels in an image), along with spot count values via internal algorithms for every sample. Spot count features were generated using the applicable IDEAS Wizards. Spot count, mean intensity, and maximum pixel ratio are calculated by (Output value with EVs/Output value without EVs).

Inhibition Assays:

EV and recipient cell co-culture was done in an environmental temperature of 4 °C. In separate wells, recipient cells were fixed prior with 4% paraformaldehyde prior to the co-culture with EVs. Both assays were compared to data from standard uptake assays.

Statistics:

All quantitative data was analyzed via GraphPad Prism 8.1.2 (San Diego, California) and done in triplicates. The data are presented as mean ± standard error of the mean (S.E.M.). Statistical significance was determined using an unpaired T-test or a One-way analysis of variance (ANOVA) with Tukey's or Dunnett's multiple comparison post-hoc compared to controls when appropriate. $p < 0.05$ was considered significant.

Results

CD63eGFP tagged HEK293T Extracellular Vesicle Properties.

To generate fluorescently labeled EVs for analyzing the kinetics and uptake of extracellular vesicles, HEK293T cells were transfected with a plasmid carrying CD63-eGFP fusion protein. CD63 is a tetraspanin protein commonly enriched in the membrane of exosomes making it an optimal target for EV fluorescent tagging (34,35). Spent media was collected from HEK293T cell culture and EVs were isolated as previously reported (8). We compared the size and distribution of EVs isolated from CD63-eGFP transfected HEK293T cells to non-transfected HEK293T cells. CD63-eGFP transfected HEK293T EVs

displayed an average median diameter of 110.28 nm and 103.616 nm respectively, as measured by nanotracking software (Fig. 1A), which is consistent with the reported size of HEK293T EVs. No significant differences in median diameter ($p = 0.1615$), distribution ($p = 0.4225$), or concentration (data not shown) of EVs isolated from non-transfected and CD63-eGFP transfected HEK293T cells were observed. eGFP labeling did not alter size of HEK293T EVs (Fig. 1B).

IFC assay was conducted to determine if the CD63-eGFP was associated with EVs. As a fluorescent negative control, 1.34 μM beads in buffer solution (Fig. 1C top), lacked fluorescence when exposed to the 488 nm excitation wavelength, but were visible in brightfield (BF) and side scatter (SSC). Untagged HEK293T EVs were negative in the BF, GFP, and SSC, suggesting a small size below the BF threshold and lack of fluorescence (Fig. 1D, middle). The absence in BF signifies an EV size smaller than 300 nm, which also suggests minimal swarming of EVs. Lastly, CD63-eGFP tagged EVs are negative in BF and positive in the GFP channel signifying positive fluorescence of the HEK293T EVs (Fig. 1C, bottom). Collectively, these results show that the isolated HEK293T EVs have standard size and protein marker profiles consistent with previous reports of HEK293T exosomes and eGFP labeling does not alter the size of HEK293T EVs (5,21).

Using a commercially available flow cytometry-based method to measure common EV markers, we determined the overall EV tetraspanin profile (5). Isolated HEK293T EVs from control and CD63-eGFP expressing HEK293T cells were positive for standard EV markers including CD9, CD63, and CD81 as measured in relative fluorescence units (Fig. 1D). As previously reported, CD29 was also found on the surface of HEK293T EVs and CD63-eGFP transfected HEK293T EVs (5). These results indicate that the isolation and tagging methods for HEK293T EV result in EVs with common HEK293T exosome markers.

2. Active uptake of EK293T EVs.

Two inhibitory internalization assays were performed. EVs were co-cultured with recipient cells at 4 °C (cold) or fixed with paraformaldehyde prior to co-culture with HEK293T EVs. The treatments decreased the presence of eGFP-labelled EVs in the recipient cells compared to recipient cells co-cultured with EVs under physiological conditions (Fig. 2A). Cold and fixed inhibitory assays reduced the spot count (Cold: $p = 0.0127$, Fixed: $p = 0.0078$), intensity (Cold: $p = 0.0105$, Fixed: $p = 0.0374$), and maximum pixel (Cold: $p = 0.0159$, Fixed: $p = 0.0149$) of fluorescence signals in recipient cells without treatments, indicating inhibition of EV uptake. These results conversely infer that eGFP localization and increases in output parameters signify that HEK293T EVs are internalized for the following uptake assays.

3. Dose dependent HEK293T EV uptake

To develop a standard dose curve for the IFC platform, HEK293T EVs were co-cultured with HEK293T recipient cells at increasing doses ranging from 0 to 20,000 EVs per cell at 37°C. Representative IFC images exhibited a visual increase of eGFP fluorescence with elevated doses of EVs (Fig. 3A). The lowest number of EVs that could be detected was 6,000 EVs per co-cultured HEK293T cell. At this level, spot count ($p = 0.0012$), intensity ($p = 0.0075$), and maximum pixel ($p = 0.0005$), measurements were

significantly greater than recipient cells without EVs (Fig. 3B-D). Therefore, doses of 6,000 HEK293T EVs is the low threshold for uptake in our experimental condition. Similarly, doses of 10,000 and 20,000 EVs had higher spot count (10,000: $p = 0.0009$; 20,000: $p < 0.0001$), intensity (10,000: $p < 0.0001$; 20,000: $p < 0.0001$), and maximum pixel (10,000: $p < 0.0001$; 20,000: $p < 0.0001$) compared to cells without EVs. Comparing between the higher doses, there are no significant differences in spot count (6,000 vs. 10,000: $p = 0.999$, 10,000 vs. 20,000: $p = 0.0927$), intensity (6,000 vs. 10,000: $p = 0.8482$, 10,000 vs. 20,000: $p = 0.999$), and maximum pixel count (6,000 vs. 10,000: $p = 0.6056$, 10,000 vs. 20,000: $p = 0.5281$) between 6,000 and 10,000, along with 10,000 vs 20,000. Similarly, comparing between 6,000 and 20,000, there is no statistical difference in spot count ($p = 0.0787$) and intensity ($p = 0.8083$). There is a significant difference in maximum pixel between 6,000 and 20,000 ($p = 0.0140$). Overall, the yield curve displays a significant dose dependence in all parameters (Spot, Intensity, Max Pixel, $p < 0.0001$). These results indicate that HEK293T EV uptake is dose dependent with a minimum threshold of 6,000 HEK293T EVs per cell.

4. HEK293T EV temporal uptake

Using 6,000 EVs per cell, HEK293T EVs were co-cultured with HEK293T cells for increasing lengths of time prior to IFC, ranging from 5 minutes to 24 hours. Length of EV exposure played a key role in the amount of visible fluorescence in the recipient cells, declining after 12 hours (Fig. 4A). Initially, 30 minutes of co-culture displayed a significant increase in spot count ($p = 0.0081$) suggesting a possible trend towards EV uptake, but not in other uptake parameters (Intensity: $p = 0.3073$, Max Pixel: $p = 0.0952$) (Fig. 4B-D). At two hours of co-culture, significantly higher spot count ($p = 0.0028$), intensity ($p = 0.0420$), and maximum pixel ($p = 0.0006$) were recorded compared to the recipient cells without EVs. Again, at 4 hours of co-culture all parameters were greater than controls (Spot count: $p = 0.0003$, Intensity: $p < 0.0001$, Max pixel: $p < 0.0001$). Intensity and maximum pixel continued to be higher than controls at 4, 12, and 24 hours of co-culture. There were no differences in any uptake parameters between 4 hours and 12 hours of co-culture (Spot: $p = 0.999$, Intensity: $p = 0.5797$ Maximum Pixel: $p = 0.2489$). However, intensity ($p = 0.0191$), and maximum pixel ($p = 0.0027$) decreased between 12 and 24 hours of co-culture (Fig. 4C-D). Similar to the dose curve, HEK293T EV uptake is time dependent with consistent EV uptake at 4 hours of incubation and a peak at 12 hours. Collectively, a dose of 6,000 EVs per cell seeded and a co-culture of 4 hours has been standardized for the following uptake assays.

5. Comparative uptake of HEK293T EVs by Multiple Cell Lines

The hypothesis that EV uptake is a selective process where EVs are preferentially taken up by cells of their own origin was tested using IFC. HEK293T EVs were co-cultured with HEK293T cells or other cell lines: epithelial (C3A liver cells), endothelial (Human Umbilical Vein Endothelial Cells), and neural (SH-SY5Y Glioblastoma Cells.). eGFP fluorescence is more abundant in HEK293T cells as compared to the other cell types (Fig. 5A). Compared to C3A and HUVECs, HEK293T cells had significantly higher fluorescence intensity (C3A: $p = 0.0321$; HUVEC: $p = 0.0055$) (Fig. 5C), when co-cultured with HEK293T EVs. Additionally, HEK293T cells had higher maximum pixel (C3A: $p = 0.0221$; HUVEC $p = 0.0079$; SH-

SY5Y: p = 0.0486) (Fig. 5D) as compared to all other recipient cell lines (Fig. 5B). Regarding intensity, SH-SY5Y cells was significantly higher than HUVECs when co-cultured with HEK293T EVs (p = 0.0304). These results support HEK293T EV selective uptake up by HEK293T cells compared to other cell lines in vitro.

6. Differentiation status of neural cells and HEK293T EV internalization

Since EVs have been implicated for therapeutic and delivery purposes targeting neural diseases, human neural stem cells (hNSCs) and mature human neurons were used as recipient cell lines in our system to examine if the differentiation status of the recipient cell plays a role in selective uptake of EVs. Representative images from IFC displayed visual evidence of uptake in both cell types, but with the greatest eGFP localization in hNSCs (Fig. 6A). hNSCs co-cultured with HEK293T EVs have higher spot count (p = 0.0082) and max pixel (p = 0.0083) as compared to mature neurons. Together, these results suggest that differentiation status of neural cells affects uptake of HEK293T EVs.

Discussion

EV in vitro uptake standardization process

A group of international experts on EVs emphasized a need to effectively determine the minimal effective dose of EVs for uptake assays and here we have developed a system that can be effectively adopted by the field (20,22,24). There are challenges when analyzing EV uptake. For example, as we and others observed, results can differ if the EV dose and exposure time are altered (20). We addressed HEK293T EV dose and concentration as a kinetic variable. Also, an in vitro minimum effective dose may more uniformly predict in vivo biodistribution of EVs and be used to develop more consistent in vivo dosing parameters for EV therapeutics and delivery. In an in vivo mouse EV biodistribution study, increasing dose of HEK293T EVs resulted in a shift of the relative EV distribution in organs (21). Similar to findings in a prior in vitro study using bladder cancer EVs (32), HEK293T EVs displayed a strong dose dependence with a minimal effective dose at 6,000 EVs in our study. We are the first to use particles per cell as a sensitive dose measurement in vitro, which better correlates with in vivo models using particles per body weight. Our data also indicated a dose saturation limit after 6,000 EVs, potentially informing future in vivo dose ranging studies by indicating that higher doses may have limited benefits.

Another potential confounding variable of measuring EV uptake is the potential temporal effects on EV uptake. In our system, we found strong time dependence with uptake as early as 2 hours with a potential decrease between 12 and 24 hours. Similar to our findings, time dependence was reported in few studies using bladder cancer cells, tumor cells, and others with uptake as early as 30 minutes through 24 hours (32,36,37). As seen with HEK293T EVs, the lower values at 24 hours of co-culture may be a result of cell division or recycling/degradation of EVs internalized at early time points (38). Specifically, since EVs have been shown to be internalized then broken down or internalized then released after 24 hours, longer incubations may generate inaccurate internalization readouts (38). Our study is the first to use IFC to provide visual and quantitative evidence of a time dependent yield curve on HEK293T EV uptake.

As the ISEV position paper suggests, the choice of an EV label may affect uptake, necessitating less disruptive techniques such as the GFP tagging methods used in our study. Specifically, 72% of researchers participating in a survey claim that lipid dye experiments are unreliable unless proper controls are used (20). EV dyes do not reliably correlate with small EV content and may even increase vesicle size. Contamination of mislabeled lipoproteins and protein content and dye aggregation contributed to false positives (39–41). Therefore, we fused CD63 with an eGFP to label the HEK293T EVs. Similar to other reports of protein tagging, HEK293T EVs were GFP positive with no observed differences in diameter and maintained standard EV surface protein composition (31,34). Despite this, it is important to note that labeling EVs with specific EV proteins may limit the tracking to only a few subtypes of EVs expressing the respective markers. Other potential limitations may be that the fluorescence intensity is dependent on protein expression level, the efficiency of EV membrane labeling, and excitation strength of the light source (42). However, IFC is sensitive, detecting low fluorescence intensity with accurate visualization of CD63-GFP particles at the 100 nm range (27,31).

Selective uptake

EVs display proteins and other signals that may confer selective uptake (18,43). Since the first step of EV biogenesis is the invagination of the plasma membrane, the EV membrane contains similar proteins, receptors, adhesion molecules, and integrins when compared with the donor cell membrane (17,18,43). The similar membrane composition leads to self-selective uptake of EVs by the donor cell type (16,17). In contrast others report that natural EVs were taken up equally by any cell type, regardless of EV origin (18,19,44) when utilizing imaging or functional knockdown assays. Using the IFC platform, we found that HEK293T extracellular vesicles are taken up at greater quantities by HEK293T cells than other reported cell lines, thus suggesting an inherent EV uptake specificity. Through this outcome and the versatility of IFC, EV sources can be appropriately selected and analyzed for targeting specific recipient cells. To our knowledge this is the first study utilizing imaging flow cytometry to analyze the specificity of HEK293T EVs.

In addition to self-selectivity, differentiation status of recipient cells has been hypothesized to play a role in uptake of EVs (45). As our group and others have shown, EVs have therapeutic effects in the central nervous system and are known to modulate cell functions in neuronal development and adults (3,7–9,46). Here for the first time, differentiation status of neurons affected EV uptake, where human neural stem cells had significantly greater uptake of HEK293T EVs compared to mature neurons. This may be a result of specific uptake mechanisms by recipient cells, where neurons endocytose EVs and the mechanism of hNSCs in this process has yet to be elucidated (38,47). However, a similar study with myeloid precursor cells found that the mature dendritic cells and macrophages internalized more EVs than immature dendritic cells and monocytes (45). The observed differences can be attributed to the phagocytic activity of further differentiated myeloid cells. Due to the in vitro evidence supporting selective uptake, HEK293T EVs can be used to modulate undifferentiated neurons in future therapeutic applications.

Conclusions

In summary, we have further developed a quantitative and high throughput platform for quantifying the kinetics of HEK293T EV uptake that can be translated to many other EV and cell types. Significantly, we found that HEK293T EV uptake is a selective process, with specificity towards HEK293T cells. The IFC assays developed here can be used to better define parameters used in in vivo dose escalation and biodistribution studies and provide instrumental information for a predictive model of EV uptake outcomes in vivo.

List Of Abbreviations

EV: extracellular vesicles, HEK293T: human embryonic kidney cell line, IFC: imaging flow cytometry, hNSC: human neural stem cell, GFP: green fluorescent protein, BF: brightfield, SSC: side scatter, ISEV: international society of extracellular vesicles

Declarations

Acknowledgements:

We would like to thank Julie Nelson of the CTEGD Cytometry Resources Lab for guidance with flow cytometry. Additionally, we would like to thank Timothy Maughon for assistance characterizing EV surface markers.

Funding:

This work was funded by the Georgia Research Alliance. ImageStreamX MKII was purchased with support from NIH (Grant: 1S10OD021719-01A1).

Author's Contributions:

BJJ organized and conducted the study. BJJ conducted statistical analysis, wrote the initial manuscript and generated appropriate figures. SLS and YY provided guidance in all aspects of the study. All authors read and approved the manuscript.

Ethics Declarations:

Ethics approval and consent to participate: Not applicable

Consent for Publication: Not applicable

Competing Interests:

SLS is a stockholder in ArunA Bio. S.L.S. was a part time employee of ArunA Bio during the study. SLS is an inventor on patent US 8,178,089 and US 7,531,354, method of producing feeder cell–free

neuroprogenitor cells, by contacting pluripotent stem cells with bFGF and a differentiation protein and assigned University of Georgia Research Foundation and exclusively licensed by ArunA Bio. SLS has a patent pending on neural exosomes, assigned University of Georgia Research Foundation, and exclusively licensed by ArunA Bio.

Availability of Data and Materials:

The datasets generated and/or analyzed during the current study are available from the corresponding author on reasonable request.

References

1. Raposo G, Stoorvogel W. Extracellular vesicles: Exosomes, microvesicles, and friends. J Cell Biol. 2013;200(4):373–83.
2. Colombo M, Raposo G, Théry C. Biogenesis, Secretion, and Intercellular Interactions of Exosomes and Other Extracellular Vesicles. Annu Rev Cell Dev Biol. 2014;30(1):255–89.
3. Webb RL, Kaiser EE, Jurgielewicz BJ, Spellicy S, Scoville SL, Thompson TA, et al. Human Neural Stem Cell Extracellular Vesicles Improve Recovery in a Porcine Model of Ischemic Stroke. Stroke. 2018;49:1248-56.
4. Marcus ME, Leonard JN. FedExosomes: Engineering Therapeutic Biological Nanoparticles that Truly Deliver. Pharmaceuticals. 2013;6:659–80.
5. Wiklander OPB, Bostancioglu RB, Welsh JA, Zickler AM, Murke F, Corso G, et al. Systematic methodological evaluation of a multiplex bead-based flow cytometry assay for detection of extracellular vesicle surface signatures. Front Immunol. 2018;9:1326.
6. Valadi H, Ekström K, Bossios A, Sjöstrand M, Lee JJ, Lötvall JO. Exosome-mediated transfer of mRNAs and microRNAs is a novel mechanism of genetic exchange between cells. Nat Cell Biol. 2007;9(6):654–9.
7. Webb RL, Kaiser EE, Scoville SL, Thompson TA, Fatima S, Pandya C, et al. Human Neural Stem Cell Extracellular Vesicles Improve Tissue and Functional Recovery in the Murine Thromboembolic Stroke Model. Transl Stroke Res. 2018;9:530–9.
8. Spellicy SE, Kaiser EE, Bowler MM, Jurgielewicz BJ, Webb RL, West FD, et al. Neural Stem Cell Extracellular Vesicles Disrupt Midline Shift Predictive Outcomes in Porcine Ischemic Stroke Model. Transl Stroke Res. 2019; https://doi.org/10.1007/s12975-019-00753-4.
9. Sun MK, Passaro AP, Latchoumane C-F, Spellicy SE, Bowler M, Goeden M, et al. Extracellular vesicles mediate neuroprotection and functional recovery after traumatic brain injury. J Neurotrauma. 2019; https://doi.org/10.1089/neu.2019.6443.
10. Ferguson S, Kim S, Lee C, Deci M, Nguyen J. The Phenotypic Effects of Exosomes Secreted from Distinct Cellular Sources: A Comparative Study based on miRNA Composition. AAPS J. 2019;20(4):67.

11. Johnsen KB, Gudbergsson JM, Skov MN, Pilgaard L, Moos T, Duroux M. A comprehensive overview of exosomes as drug delivery vehicles — Endogenous nanocarriers for targeted cancer therapy. Biochim Biophys Acta - Rev Cancer. 2014;1846(1):75–87.
12. Faruqu FN, Xu L, Al-Jamal KT. Preparation of Exosomes for siRNA Delivery to Cancer Cells. J Vis Exp. 2018;(142):doi:10.3791/58814.
13. Kooijmans SAA, Stremersch S, Braeckmans K, De Smedt SC, Hendrix A, Wood MJA, et al. Electroporation-induced siRNA precipitation obscures the efficiency of siRNA loading into extracellular vesicles. J Control Release. 2013;172:229–38.
14. Mizrak A, Fatih Bolukbasi M, Baris Ozdener G, Brenner GJ, Madlener S, Pekcan Erkan E, et al. Genetically Engineered Microvesicles Carrying Suicide mRNA/Protein Inhibit Schwannoma Tumor Growth. Mol Ther. 2013;21:101–8.
15. Ohno S, Takanashi M, Sudo K, Ueda S, Ishikawa A, Matsuyama N, et al. Systemically Injected Exosomes Targeted to EGFR Deliver Antitumor MicroRNA to Breast Cancer Cells. Mol Ther. 2013;21(1):185–91.
16. Rana S, Yue S, Stadel D, Zöller M. Toward tailored exosomes: The exosomal tetraspanin web contributes to target cell selection. Int J Biochem Cell Biol. 2012;44:1574–84.
17. Sancho-Albero M, Navascués N, Mendoza G, Sebastián V, Arruebo M, Martín-Duque P, et al. Exosome origin determines cell targeting and the transfer of therapeutic nanoparticles towards target cells. J Nanobiotechnology. 2019;17(1):16.
18. Mulcahy LA, Pink RC, Raul D, Carter F, David D, Carter RF. Routes and mechanisms of extracellular vesicle uptake. J Extracell Vesicles. 2014;3(24641).
19. Zech D, Rana S, Büchler MW, Zöller M. Tumor-exosomes and leukocyte activation: an ambivalent crosstalk. 2012;10(37):https://doi.org/10.1186/1478-811X-10-37.
20. Russell AE, Sneider A, Witwer KW, Bergese P, Bhattacharyya SN, Cocks A, et al. Biological membranes in EV biogenesis, stability, uptake, and cargo transfer: an ISEV position paper arising from the ISEV membranes and EVs workshop. J Extracell Vesicles. 2019;8(1):1684862.
21. Wiklander OPB, Nordin JZ, O'Loughlin A, Gustafsson Y, Corso G, Mäger I, et al. Extracellular vesicle in vivo biodistribution is determined by cell source, route of administration and targeting. J Extracell vesicles. 2015;4:26316.
22. Busatto S, Giacomini A, Montis C, Ronca R, Bergese P. Uptake Profiles of Human Serum Exosomes by Murine and Human Tumor Cells through Combined Use of Colloidal Nanoplasmonics and Flow Cytofluorimetric Analysis. Anal Chem. 2018;90:7861.
23. Feng D, Zhao WL, Ye YY, Bai XC, Liu RQ, Chang LF, et al. Cellular internalization of exosomes occurs through phagocytosis. Traffic. 2010 May;11(5):675–87.
24. Mastoridis S, Bertolino GM, Whitehouse G, Dazzi F, Sanchez-Fueyo A, Martinez-Llordella M. Multiparametric Analysis of Circulating Exosomes and Other Small Extracellular Vesicles by Advanced Imaging Flow Cytometry. Front Immunol. 2018;9:1583.

25. Hazan-Halevy I, Rosenblum D, Weinstein S, Bairey O, Raanani P, Peer D. Cell-specific uptake of mantle cell lymphoma-derived exosomes by malignant and non-malignant B-lymphocytes HHS Public Access. Cancer Lett. 201;364(1):59–69.
26. Corso G, Mäger I, Lee Y, Görgens A, Bultema J, Giebel B, et al. Reproducible and scalable purification of extracellular vesicles using combined bind-elute and size exclusion chromatography. Sci Rep. 2017;7(1)11561.
27. Ricklefs FL, Maire CL, Reimer R, Dührsen L, Kolbe K, Holz M, et al. Imaging flow cytometry facilitates multiparametric characterization of extracellular vesicles in malignant brain tumours. J Extracell Vesicles. 2019;8(1)1588555.
28. Gomes J, Lucien F, Cooper TT, Kim Y, Williams KC, Liao X, et al. Analytical Considerations in Nanoscale Flow Cytometry of Extracellular Vesicles to Achieve Data Linearity. Thromb Haemost. 2018;118(09):1612–24.
29. Lannigan J, Erdbruegger U. Imaging flow cytometry for the characterization of extracellular vesicles. Methods. 2017;112:55–67.
30. Erdbrügger U, Rudy CK, E. Etter M, Dryden KA, Yeager M, Klibanov AL, et al. Imaging flow cytometry elucidates limitations of microparticle analysis by conventional flow cytometry. Cytom Part A. 2014;85(9):756–70.
31. Görgens A, Bremer M, Ferrer-Tur R, Murke F, Tertel T, Horn PA, et al. Optimisation of imaging flow cytometry for the analysis of single extracellular vesicles by using fluorescence-tagged vesicles as biological reference material. J Extracell Vesicles. 2019;8(1):1587567.
32. Franzen CA, Simms PE, Van Huis AF, Foreman KE, Kuo PC, Gupta GN. Characterization of uptake and internalization of exosomes by bladder cancer cells. Biomed Res Int.2014: 619829.
33. Ofir-Birin Y, Abou karam P, Rudik A, Giladi T, Porat Z, Regev-Rudzki N. Monitoring Extracellular Vesicle Cargo Active Uptake by Imaging Flow Cytometry. Front Immunol. 2018;9:1011.
34. Mittelbrunn M, Gutiérrez-Vázquez C, Villarroya-Beltri C, González S, Sánchez-Cabo F, González MÁ, et al. Unidirectional transfer of microRNA-loaded exosomes from T cells to antigen-presenting cells. Nat Commun. 2011;2(1):282.
35. Chivet M, Javalet C, Laulagnier K, Blot B, Hemming FJ, Sadoul R. Exosomes secreted by cortical neurons upon glutamatergic synapse activation specifically interact with neurons. J Extracell Vesicles. 2014;3(1):24722.
36. Escrevente C, Keller S, Altevogt P, Costa J. Interaction and uptake of exosomes by ovarian cancer cells. BMC Cancer. 2011;11(1):108.
37. Schneider DJ, Speth JM, Penke LR, Wettlaufer SH, Swanson JA, Peters-Golden M. Mechanisms and modulation of microvesicle uptake in a model of alveolar cell communication. J Biol Chem. 2017;292(51):20897–910.
38. Polanco JC, Li C, Durisic N, Sullivan R, Götz J. Exosomes taken up by neurons hijack the endosomal pathway to spread to interconnected neurons. Acta Neuropathol Commun. 2018;6(1):10.

39. Takov K, Yellon DM, Davidson SM. Confounding factors in vesicle uptake studies using fluorescent lipophilic membrane dyes. J Extracell Vesicles. 2017;6(1):1388731.
40. Pužar Dominkuš P, Stenovec M, Sitar S, Lasič E, Zorec R, Plemenitaš A, et al. PKH26 labeling of extracellular vesicles: Characterization and cellular internalization of contaminating PKH26 nanoparticles. Biochim Biophys Acta - Biomembr. 2018;1860(6):1350–61.
41. Dehghani M, Gulvin SM, Flax J, Thomas R. Exosome labeling by lipophilic dye PKH26 results in significant increase in vesicle size. BioRxiv. 2019;https://doi.org/10.1101/532028.
42. Chuo ST-Y, Chien JC-Y, Lai CP-K. Imaging extracellular vesicles: current and emerging methods. J Biomed Sci. 2018;25(1):91.
43. Mathieu M, Martin-Jaular L, Lavieu G, Théry C. Specificities of secretion and uptake of exosomes and other extracellular vesicles for cell-to-cell communication. Nat Cell Biol . 2019;21(1):9–17.
44. Alvarez-Erviti L, Seow Y, Yin H, Betts C, Lakhal S, A Wood MJ. Delivery of siRNA to the mouse brain by systemic injection of targeted exosomes. Nature Biotech. 2011;29:341-345.
45. Czernek L, Chworos A, Duechler M. The Uptake of Extracellular Vesicles is Affected by the Differentiation Status of Myeloid Cells. Scand J Immunol. 2015;82(6):506–14.
46. Hong S-B, Yang H, Manaenko A, Lu J, Mei Q, Hu Q. Potential of Exosomes for the Treatment of Stroke. Cell Transplant. 2019;28(6):662–70.
47. Janas AM, Sapoń K, Janas T, Stowell MHB, Janas T. Exosomes and other extracellular vesicles in neural cells and neurodegenerative diseases. Biochim Biophys Acta - Biomembr. 2016;1858(6):1139–51.

Figures

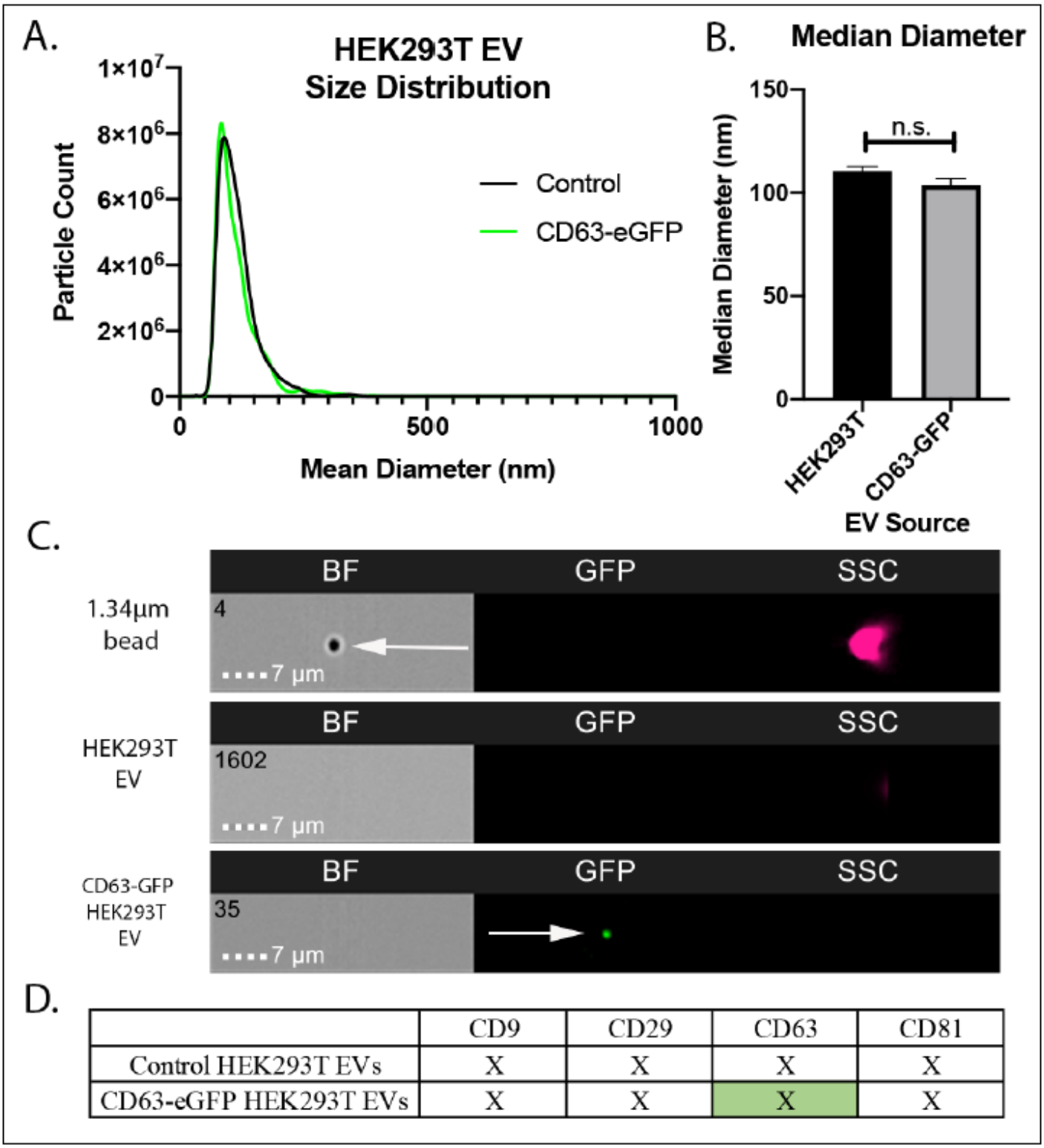

	CD9	CD29	CD63	CD81
Control HEK293T EVs	X	X	X	X
CD63-eGFP HEK293T EVs	X	X	X	X

Figure 1

Characterization of HEK293T EVs tagged with CD63-eGFP. EVs were isolated from HEK293T (control) and HEK293T expressing CD63-eGFP cell culture media. A. Representative EV size distribution recorded via nanotracking software. B. Quantification of mean diameter distribution of transfected vs. non-transfected HEK293T EVs. C. IFC images of negative control beads, HEK293T control EVs, and CD63-eGFP tagged EVs. BF signifies Brightfield, GFP signifies green fluorescent protein (488nm excitation laser) and SSC

signifies side scatter. Positive eGFP in GFP channel signifies fluorescent HEK293T EVs. D. Flow cytometry based MACSPlex surface marker expression of non-transfected HEK293T EVs and HEK293T CD63-eGFP EVs. Both EV sources are positive for CD29, CD9, CD63, and CD81, as measured in relative fluorescence (denoted by X for positive). Bars represent mean ± SEM; N = 3; unpaired T-test. n.s. signifies p>0.05

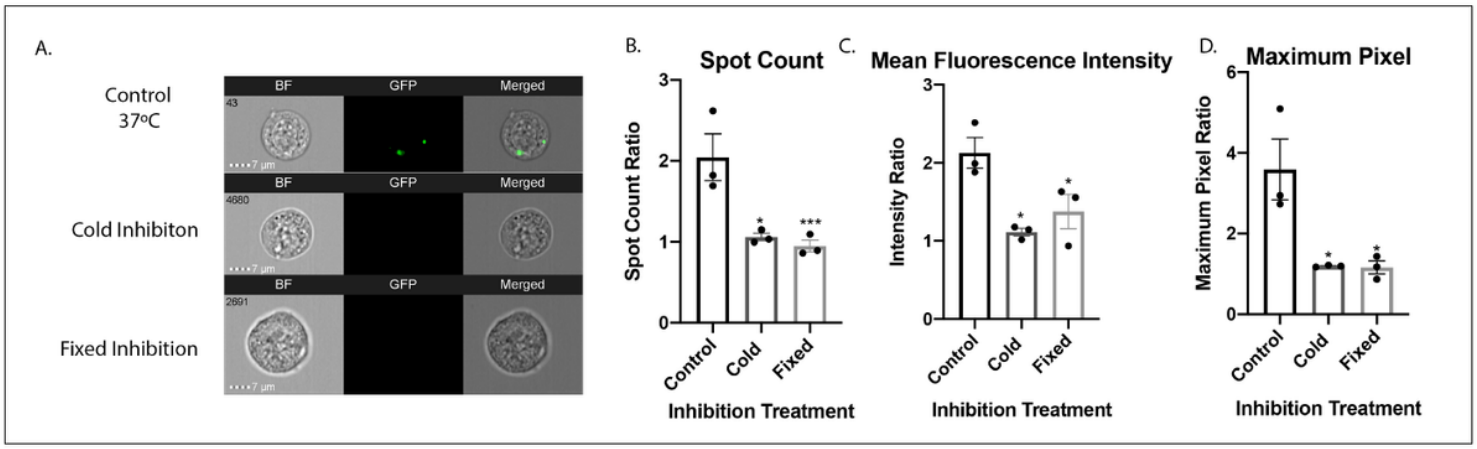

Figure 2

EV internalization inhibition assays. HEK293T cells were co-cultured with HEK293T EVs under various conditions. Control (37□C) refers to co-culture in physiological 37□C environment. Cold refers to co-culture in a 4□C environment. Fixed inhibition refers to an assay where recipient cells were PFA fixed prior to co-culture. A. Representative IFC images of recipient cells. Column 1, BF, signifies bright field. Column 2, GFP, signifies green fluorescent protein (488nm excitation laser), and Column 3 signifies a merge of BF and GFP. Control shows positive GFP representing EV internalization. B-D. Quantification of inhibition assays compared to controls via spot count, mean fluorescence intensity, and maximum pixel. Bars represent mean ± SEM; N = 3; one-way ANOVA followed with Tukey's post hoc test compared to control. *p<0.05 ***p<0.01

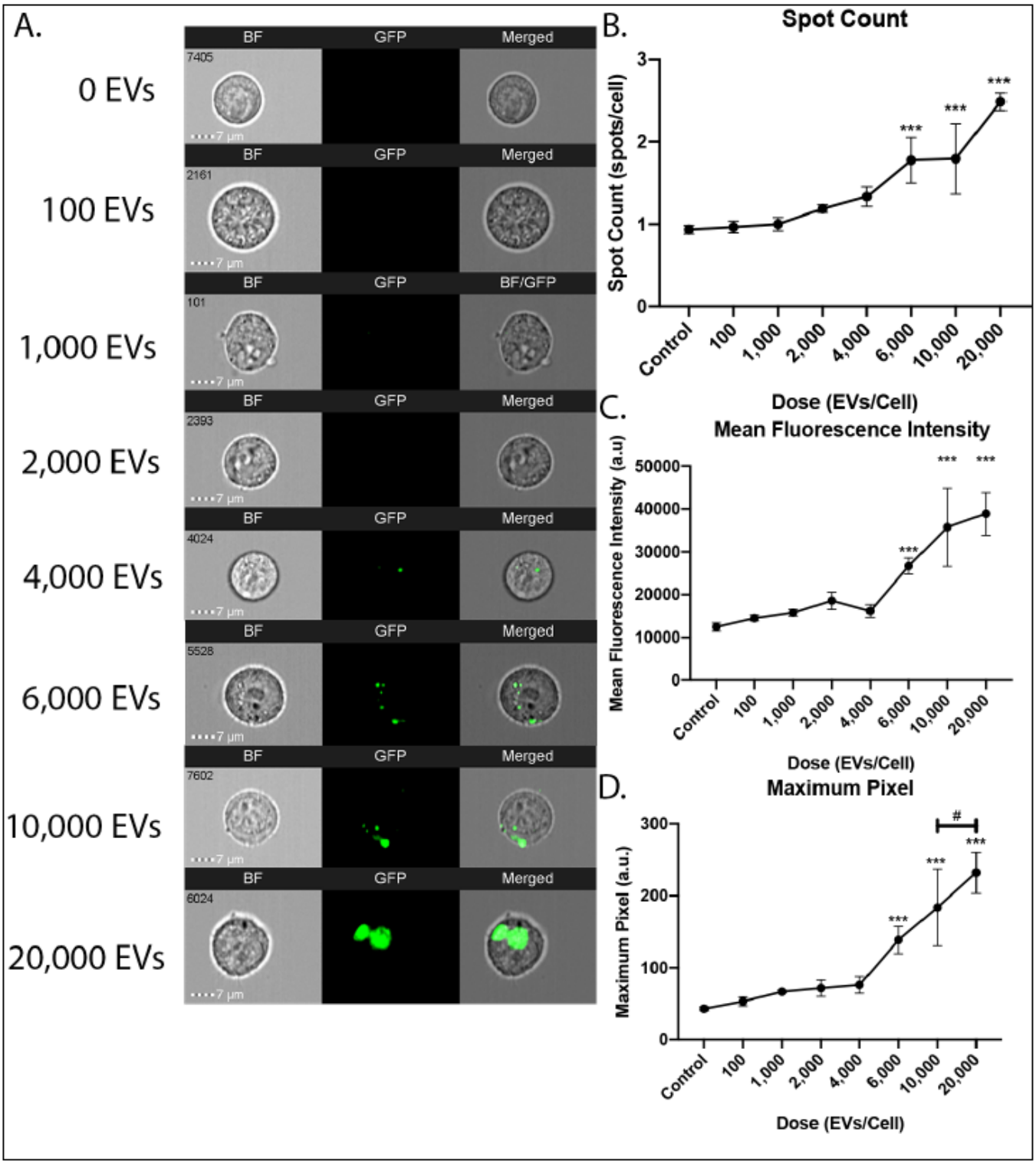

Figure 3

HEK293T EV uptake has a dose effect with a minimum threshold of 6,000EVs. HEK293T cells were co-cultured with HEK293T EVS at increasing doses from 0-20,000/cell. A. Representative IFC images of recipient cells with respective EV doses. GFP localization signifies HEK293T EV uptake. B-D. Quantification of dose assays compared to controls and each group via spot count, mean fluorescence

intensity, and maximum pixel ratios. Bars represent mean ± SEM; N = 3; one-way ANOVA followed with Tukey's post hoc test. *p<0.05 ***p<0.01

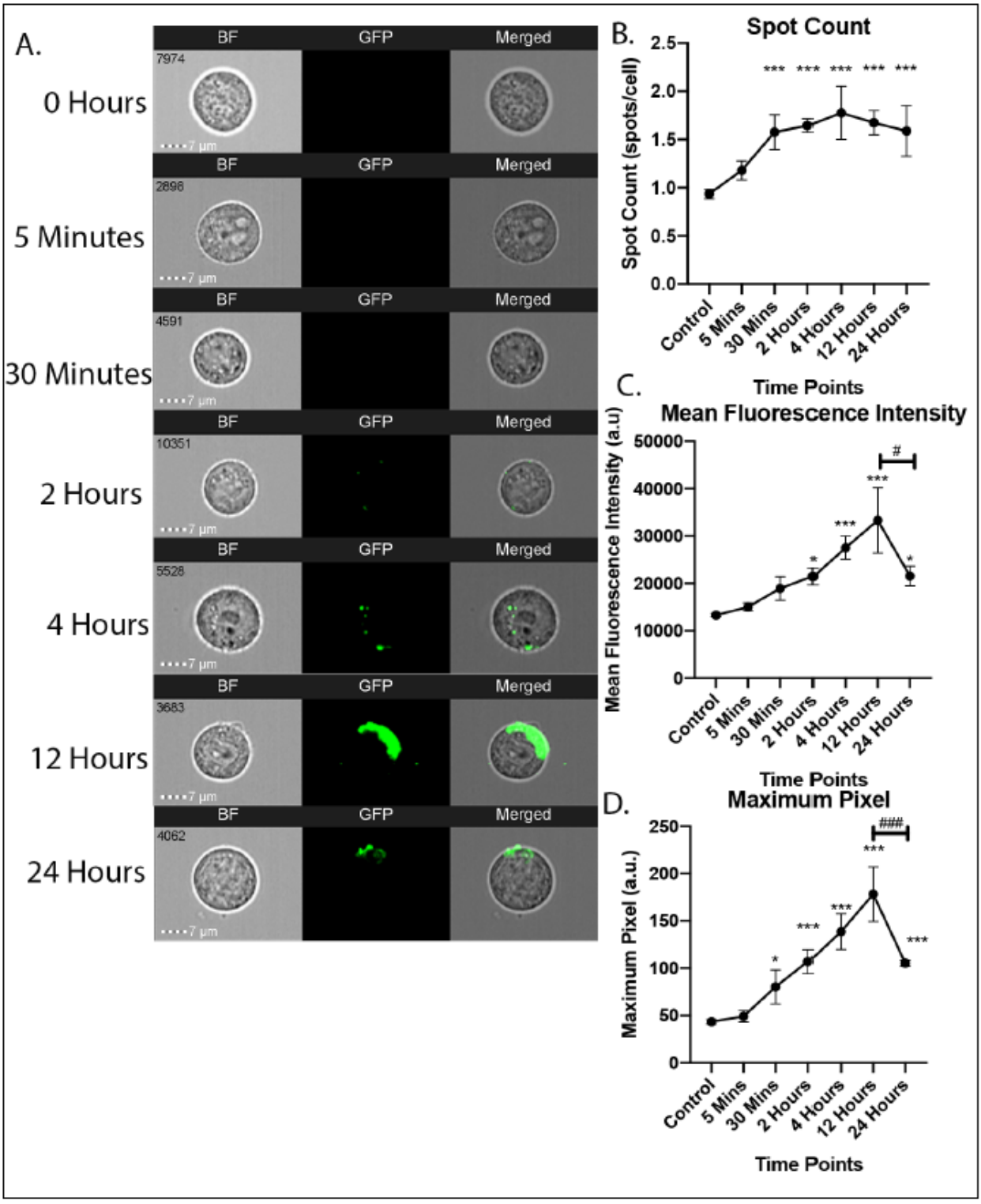

Figure 4

HEK293T EV uptake is time dependent. HEK293T cells were co-cultured with 6,000 HEK293T EVs/cell for increasing lengths of time. A. Representative IFC images of recipient cells respectively. GFP localization signifies increased HEK293T EV uptake. B-D. Quantification of time course assays compared to controls

and each group via spot count, mean fluorescence intensity, and maximum pixel ratios. Bars represent mean ± SEM; N = 3; one-way ANOVA followed with Tukey's post hoc test. *p<0.05 ***p<0.01

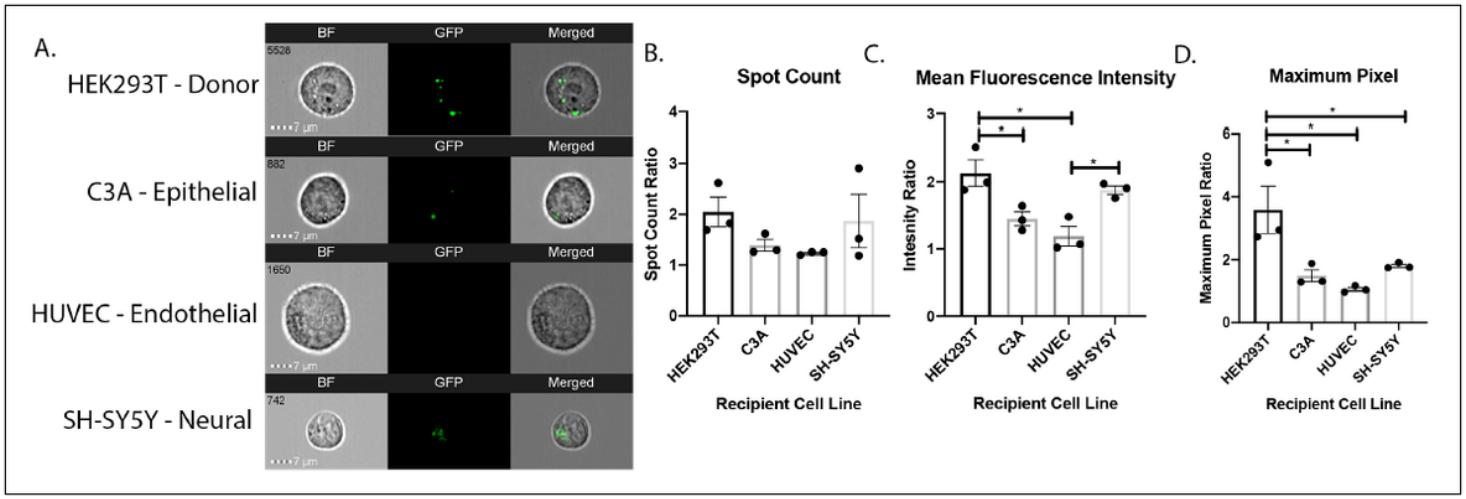

Figure 5

HEK293T EVs display uptake preference to HEK293T cells. HEK293T EVs were co-cultured with HEK293T cells, C3A epithelial cells, human umbilical vein endothelial cells (HUVEC), and SY5Y neural cells. A. Representative IFC images of recipient cells co-cultured with HEK293T EVs. B-D. Quantification of EV uptake preference assays compared to controls and each other via spot count, mean fluorescence intensity, and maximum pixel ratios. Bars represent mean ± SEM; N = 3; one-way ANOVA followed with Tukey's post hoc test. *p<0.05 ***p<0.01

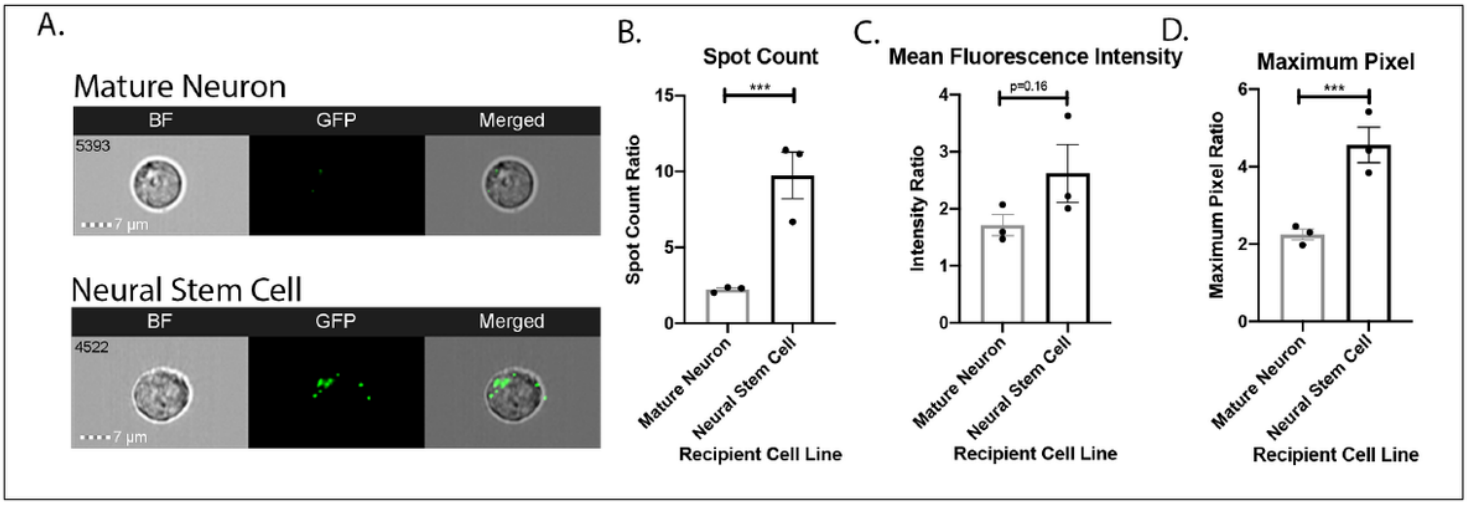

Figure 6

Neural differentiation status affects HEK293T EV uptake. HEK293T EVs were co-cultured with mature human neurons and human neural stem cells. A. Representative IFC images of recipient cells co-cultured with HEK293T EVs. B-D. Quantification of EV uptake preference assays compared to controls and each other via spot count, mean fluorescence intensity, and maximum pixel ratios. Bars represent mean ± SEM; N = 3; unpaired T-Test. *p<0.05 ***p<0.01 compared to 0 EVs (control).